

Central Schemes and Second Order Boundary Conditions for 1D Interface and Piston Problems in Lagrangian Coordinates

Riccardo Fazio^{1,*} and Giovanni Russo²

¹ *Department of Mathematics, University of Messina, Salita Sperone 31, 98166 Messina, Italy.*

² *Department of Mathematics and Computer Science, University of Catania, Viale Andrea Doria 6, 95125 Catania, Italy.*

Received 31 January 2009; Accepted (in revised version) 22 January 2010

Communicated by Eitan Tadmor

Available online 17 May 2010

Abstract. We study high-resolution central schemes in Lagrangian coordinates for the one-dimensional system of conservation laws describing the evolution of two gases in slab geometry separated by an interface. By using Lagrangian coordinates, the interface is transformed to a fixed coordinate in the computational domain and, as a consequence, the movement of the interface is obtained as a byproduct of the numerical solution. The main contribution is the derivation of a special equation of state to be imposed at the interface in order to avoid non-physical oscillations. Suitable boundary conditions at the piston that guarantee second order convergence are described.

We compare the solution of the piston problem to other results available in the literature and to a reference solution obtained within the adiabatic approximation. A shock-interface interaction problem is also treated. The results on these tests are in good agreement with those obtained by other methods.

AMS subject classifications: 65M06, 65M99, 76T05

Key words: Lagrangian central schemes, Euler equations, interface conditions, boundary conditions.

1 Introduction

The numerical simulation of interface and multi-fluid problems is a research topic of relevant interest in several branches of the applied sciences. To mention some issues, we

*Corresponding author. *Email addresses:* rfazio@dipmat.unime.it (R. Fazio), russo@dmi.unict.it (G. Russo)

have: bubble evolution in nuclear flows, combustion applications, chemical reactions, etc.

We study high-resolution central schemes for the one-dimensional system of conservation laws describing the evolution of two gases in slab geometry separated by an interface, using the equations in Lagrangian form. By using Lagrangian coordinates, the interface is transformed to a fixed coordinate in the computational domain and, as a consequence, the movement of the interface is obtained as a byproduct of the numerical solution. The idea to apply a Lagrangian method to interface problems is not new and for a survey on this subject we refer to the one by Benson [4].

The difficulties to retain pressure equilibrium at the interface has been indicated as the main reason for the failure of many successful single component schemes when applied to multi-component problems by several authors (see the review article by Abgrall and Karni [3] and the references quoted therein). A solution to this problem has been to use the pressure equation in the cells near the interface, as proposed by Karni [13] and investigated by Abgrall [2]. In this way the scheme is not entirely conservative, but lack of conservation, that can be checked *a posteriori*, is quite small. A similar approach has been used by Fedkiw *et al.* [10] in the context of multi-fluid flows, see also the book by Osher and Fedkiw [21, Ch. 15] and the references quoted therein, and by Wang *et al.* [23] within a mass conservation principle. Recent studies, for instance by Brummelen and Koren [22] or by Lombard and Donat [18], have proposed conservative and pressure-invariant methods enforcing zero or even first order jump conditions at the interface. The intrinsic difficulty related to the evolution of the interface has induced some authors, Davis [5] and Fazio and LeVeque [8], to apply an exact Riemann solver at the interface to find an approximation of its velocity. In particular, in paper [8] the authors use a moving mesh to enforce that the interface and the piston lie at cell edges.

Here we propose the use of a central scheme on a staggered grid, which is conservative and does not require the solution to exact or approximate Riemann problems. Furthermore, by using Lagrangian coordinates, we do not require the use of additional equations for the interface motion, as is done, for example, with level set methods (see Mulder *et al.* [19]) or mass fraction models (see Abgrall [1] and Larouturou [16]). The choice of the staggered grid is motivated by the higher resolution of such schemes with respect to the corresponding non-staggered version of the same order [15]. Of course it is possible to improve the resolution of second order central schemes on non staggered grids, but this requires more sophisticated approaches [14].

The choice of a staggered central scheme for the treatment of an interface may be questionable, because of the unavoidable smearing introduced by the staggered approach, as opposed to non staggered upwind schemes that provide a much better resolution of the interface. However, here we want to show that with a suitable choice of an interface condition, staggered central schemes are robust enough to be able to treat interfaces, maintaining a reasonable resolution.

Our scheme is based on the derivation of a suitable equation of state for the pressure to be used in the cell containing the interface. Preliminary work on this subject has been

presented to the 8th International Hyperbolic Conference held in Magdeburg [9] where the Lagrangian treatment of the interface has been introduced, and to the ENUMATH Conference held in Ischia [7] where a comparison between Lagrangian approach and Eulerian formulation with moving mesh is presented.

The main contribution of this paper consists in the second order treatment of the boundary conditions, and in the comparison of the results with those obtained by methods based on Eulerian formulation and moving mesh. Furthermore, the treatment of the interface is explained with greater detail than in previous work.

To validate the scheme we perform several tests and compare the results with those obtained by other methods. In particular we consider the piston problem treated by Fazio and LeVeque [8], a reference solution of the equation of motion of the piston in the adiabatic approximation, and a shock-interface interaction problem of Abgrall and Karni [3]. Other numerical tests can be found in the quoted conference proceedings [9] and [7].

For piston problems, a detailed description of the boundary conditions at the piston is provided. The new boundary condition is obtained by applying the piston equation of motion on the boundary, and by the use of the adiabaticity condition at the piston. It is shown that the usual reflecting boundary conditions, although consistent with the governing equations, lead to a degradation of the accuracy.

The plan of the paper is the following. Next section is devoted to the physical description of the problem, and to the equations in Lagrangian coordinates. In Section 3 we consider the piston problem for a single gas. After a brief review of the Nessyahu-Tadmor scheme, we describe in detail how to implement second order boundary conditions at the piston. The last part of the section is devoted to numerical tests on a single gas piston problem.

In Section 4 we describe the equation of state for the cell containing the interface. Section 5 contains several numerical tests for two fluid problems, solved by the new scheme and compared with adiabatic limits and solutions obtained by other methods. In the last section we draw some conclusions.

2 Description of the problem

In this section we introduce an interface problem involving a moving piston at one boundary and as a special case a classical tube problem with an interface and fixed boundaries.

2.1 Interface and piston problems

We consider first a piston problem in which the tube contains two different gases separated by a contact discontinuity at some point $I(t) < L(t)$, where $I(t)$ and $L(t)$ represent the interface between the two gases and piston position respectively (see Fig. 1).

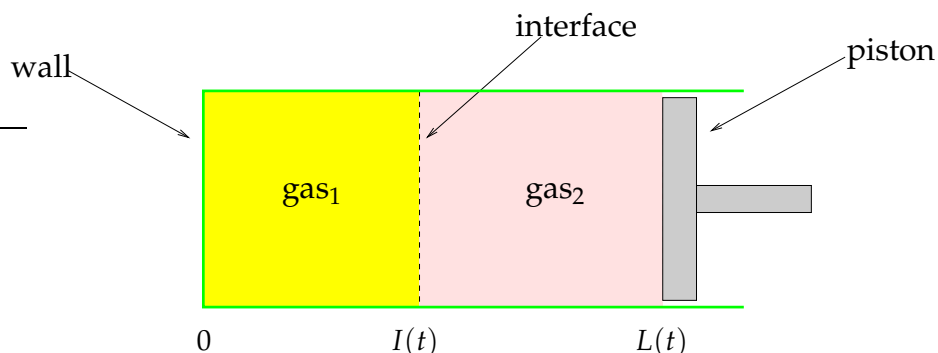


Figure 1: Physical setup for the piston problem.

The governing equations are Euler equations of gas dynamics, that is

$$\frac{\partial \mathbf{q}}{\partial t} + \frac{\partial}{\partial x} [\mathbf{f}(\mathbf{q})] = \mathbf{0}, \quad (2.1)$$

with

$$\mathbf{q} = [\rho, \rho u, E]^T, \quad (2.2a)$$

$$\mathbf{f}(\mathbf{q}) = [\rho u, \rho u^2 + p, (E + p)u]^T, \quad (2.2b)$$

and with the constitutive law for ideal gases

$$p = (\gamma(x, t) - 1) \left(E - \frac{1}{2} \rho u^2 \right), \quad (2.3)$$

where ρ , u , E , and p denote density, velocity, total energy density per unit volume, and pressure of the gas. The polytropic constant $\gamma(x, t)$ takes the value γ_1 on $0 \leq x < I(t)$, and γ_2 on $I(t) < x \leq L(t)$. The motion of the piston is driven by Newton's equation

$$\frac{d^2 L}{dt^2} = \frac{A}{m} \left(p(L(t), t) - p_{out}(t) \right), \quad (2.4)$$

where A is the area of the piston, m is its mass and $p_{out}(t)$ is the external pressure.

Next we consider the classical tube problem with an interface and fixed boundaries which is a particular case of the previous, obtained by setting $A = 0$.

2.2 Lagrangian formulation

By introducing the Lagrangian coordinate ζ given by

$$\zeta = \int_0^x \rho(z, t) dz,$$

the Euler equations (2.1)-(2.2) can be transformed in Lagrangian form

$$\frac{D\mathbf{q}}{Dt} + \frac{\partial}{\partial \xi} [\mathbf{f}(\mathbf{q})] = \mathbf{0}, \tag{2.5}$$

which is also in conservation form with

$$\mathbf{q} = [V, u, \mathcal{E}]^T, \tag{2.6a}$$

$$\mathbf{f}(\mathbf{q}) = [-u, p, up]^T, \tag{2.6b}$$

here the time derivative is the Lagrangian derivative

$$\frac{D}{Dt} = \frac{\partial}{\partial t} + u \frac{\partial}{\partial x},$$

the new field variables are defined by $V(\xi, t) = \rho^{-1}$, $\mathcal{E} = E/\rho$, and the equation of state (2.3) becomes

$$p = (\gamma(\xi, t) - 1) \left(\mathcal{E} - \frac{1}{2}u^2 \right) / V. \tag{2.7}$$

Note that the total mass

$$\xi_{\max} = \int_0^{L(t)} \rho(z, t) dz,$$

is constant.

The inverse transformation of coordinate is given by

$$x = \int_0^{\xi} V(z, t) dz. \tag{2.8}$$

The interval $0 \leq \xi \leq \xi_{\max}$ will be our "computational domain" in which we have a fixed uniform grid with $\xi_j = (j - 1/2)\Delta\xi$ for $j = 1, 2, \dots, J$ denoting the center of j -th cell, and $\Delta\xi = \xi_{\max}/J$. System (2.5)-(2.6) has three eigenvalues, $\lambda = (-c_{\text{Lag}}, 0, c_{\text{Lag}})$, where c_{Lag} is the sound speed (in Lagrangian coordinates).

Note that the sound speed for a polytropic gas in Lagrangian coordinates takes the form $c_{\text{Lag}} = \sqrt{\gamma p/V}$, which is different from the usual sound speed in Eulerian coordinates, $c_s = \sqrt{\gamma p/\rho}$. This is not surprising, because the relation between the infinitesimal distance between two material points in Eulerian and Lagrangian coordinates is given by $dx = (\partial x/\partial \xi)d\xi = V d\xi$ and therefore the ratio between the two sound speeds is given by the Jacobian of the transformation.

2.3 Boundary conditions

We would like to spend a few words about the boundary conditions at the edges of the computational domain.

At the left edge, we use standard boundary conditions for a wall, namely

$$u = u_b, \quad \frac{\partial p}{\partial x} = 0, \quad \frac{\partial \rho}{\partial x} = 0, \quad (2.9)$$

where u_b denotes the wall velocity (in our case $u_b = 0$).

The condition on the velocity is obvious, since at the wall the gas has the same velocity of the boundary. The other two conditions can be deduced by a symmetry argument, by considering that a wall is equivalent to having a symmetric gas configuration on the other side of it. This symmetry consideration no longer applies on the moving boundary, if the speed of the piston is not constant. In this case one has to resort to other conditions.

On the moving boundary, the velocity of the gas is equal to piston velocity. Direct compatibility of the boundary condition on the velocity with momentum conservation law, which is

$$\frac{Du}{Dt} + \frac{\partial p}{\partial \xi} = 0, \quad (2.10)$$

gives

$$\frac{\partial p}{\partial \xi} = -\frac{d^2 L}{dt^2}. \quad (2.11)$$

The condition on the density can be obtained by observing that, for smooth flows, the entropy is constant at material lines, i.e.,

$$\frac{DS}{Dt} = 0.$$

This implies that if

$$\left. \frac{\partial S}{\partial x} \right|_{x=L(0)} = 0,$$

then

$$\left. \frac{\partial S}{\partial x} \right|_{x=L(t)} = 0.$$

This latter equation is obtained by differentiating the evolution equation for the entropy density. In fact, let $S' \equiv \partial S / \partial x$; differentiating the equation

$$\frac{\partial S}{\partial t} + u \frac{\partial S}{\partial x} = 0$$

with respect to space one obtains

$$\frac{DS'}{Dt} = -S' \frac{\partial u}{\partial x},$$

which shows that on the boundary it is $S'(t) = 0$ if $S'(0) = 0$.

This condition, expressed in Eulerian coordinates, becomes

$$\frac{\partial \rho}{\partial x} = \frac{1}{c_s^2} \frac{\partial p}{\partial x'}$$

where $c_s^2 = (\partial p / \partial \rho)_S$ is the square of the sound speed. In Lagrangian coordinates, this relation reads

$$\left. \frac{\partial p}{\partial V} \right|_S \frac{\partial V}{\partial \xi} = \frac{\partial p}{\partial \xi'} \tag{2.12}$$

where $c_{Lag}^2 = -(\partial p / \partial V)_S$ is the square of the sound speed in Lagrangian coordinates. For a polytropic gas, this condition states that, at the boundary,

$$\gamma \frac{p}{V} \frac{\partial V}{\partial \xi} = \frac{\partial p}{\partial \xi'} \tag{2.13}$$

This formulation of piston boundary conditions is general; here we use it with the Lagrangian formulation, but it can be used in the treatment of the piston based on the Eulerian formulation with moving mesh.

Remark 2.1. The boundary conditions on pressure and density are very similar to the so-called first-order jump condition at material interfaces used by Lombard and Donat [18]:

$$\left[\left[\frac{1}{\rho} \frac{\partial p}{\partial x} \right] \right] = 0, \quad \left[\left[\rho c_s^2 \frac{\partial u}{\partial x} \right] \right] = 0, \tag{2.14}$$

where $[[\cdot]]$ is the jump operator. Such conditions can be in fact deduced as follows: Eq. (2.10) holds on both sides of the interface. The first term represents the fluid particle acceleration, which is continuous across the interface, because the latter is a material point. As a consequence one obtains

$$\left[\left[\frac{\partial p}{\partial \xi} \right] \right] = 0,$$

which is the first condition of (2.14). The second condition is obtained as follows. From the conservation of mass one has

$$\frac{D\rho}{Dt} + \rho u_x = 0,$$

and, because the entropy density is constant on material lines, one obtains

$$\frac{Dp}{Dt} + \rho c_s^2 u_x = 0.$$

Second condition (2.14) is then obtained by continuity of the pressure across the interface.

As in our case, the jump conditions are a direct consequence of the governing equations (2.5)-(2.6).

Remark 2.2. The numerical boundary conditions can be obtained by discretizing the above relations (2.11)-(2.12) at the boundaries. Using conditions of the form (2.9) instead of (2.11)-(2.12) for pressure and density also at the piston boundary produces an error which is first order in the space step, therefore the scheme is still consistent to the equations, but the accuracy is degraded.

3 Staggered central discretization

3.1 The Nessyahu and Tadmor central scheme

The Nessyahu and Tadmor central scheme [20] has the form of a predictor-corrector scheme

$$\begin{aligned} \mathbf{q}_j^{n+1/2} &= \mathbf{q}_j^n - \frac{\mu}{2} \mathbf{f}'_j, \\ \mathbf{q}_{j+1/2}^{n+1} &= \frac{1}{2}(\mathbf{q}_j^n + \mathbf{q}_{j+1}^n) + \frac{1}{8}(\mathbf{q}'_j - \mathbf{q}'_{j+1}) - \mu \left(\mathbf{f}(\mathbf{q}_{j+1}^{n+1/2}) - \mathbf{f}(\mathbf{q}_j^{n+1/2}) \right), \end{aligned}$$

where \mathbf{q}_j^n denotes an approximation of the cell average of the field at time t_n

$$\mathbf{q}_j^n \approx \frac{1}{\Delta \xi} \int_{\xi_j - \Delta \xi/2}^{\xi_j + \Delta \xi/2} \mathbf{q}(\xi, t_n) d\xi,$$

$\mu = \Delta t / \Delta \xi$ and $\mathbf{q}'_j / \Delta \xi$ and $\mathbf{f}'_j / \Delta \xi$ are a first order approximation of the space derivatives of the field and of the flux and can be computed in several ways. The simplest choice is

$$\begin{aligned} \mathbf{q}'_j &= \text{MM}(\mathbf{q}_{j+1} - \mathbf{q}_j, \mathbf{q}_j - \mathbf{q}_{j-1}), \\ \mathbf{f}'_j &= \text{MM}(\mathbf{f}_{j+1} - \mathbf{f}_j, \mathbf{f}_j - \mathbf{f}_{j-1}), \end{aligned}$$

where $\text{MM}(v, w)$ is the min-mod limiter

$$\text{MM}(v, w) = \begin{cases} \text{sgn}(v) \cdot \min(|v|, |w|), & \text{if } \text{sgn}(v) = \text{sgn}(w), \\ 0, & \text{otherwise.} \end{cases}$$

This limiter, however, may cause a degradation of accuracy near local extrema (clipping phenomena). In order to avoid this effect we use the UNO limiter proposed by Harten [12]

$$w'_j = \text{MM} \left(d_{j-1/2} + \frac{1}{2} \text{MM}(D_{j-1}, D_j), d_{j+1/2} - \frac{1}{2} \text{MM}(D_j, D_{j+1}) \right), \quad (3.1)$$

where

$$d_{j+1/2} = \bar{w}_{j+1} - \bar{w}_j, \quad D_j = \bar{w}_{j+1} - 2\bar{w}_j + \bar{w}_{j-1}.$$

Several other choices of the limiters are possible, as discussed in [20].

The time step Δt must satisfy the stability condition

$$\mu \max_j \rho(A(\mathbf{q}_j^n)) \leq \frac{1}{2},$$

where $\rho(A)$ denotes the spectral radius of the Jacobian matrix

$$A = \left[\frac{\partial f_i}{\partial q_k} \right].$$

This condition ensures that the generalized Riemann problems with piece-wise smooth data at time t_n do not interact during the time step Δt .

We note that after one time step, the numerical solution is computed on a staggered grid (see Fig. 2). After two time steps the numerical solution is evaluated on the original grid.

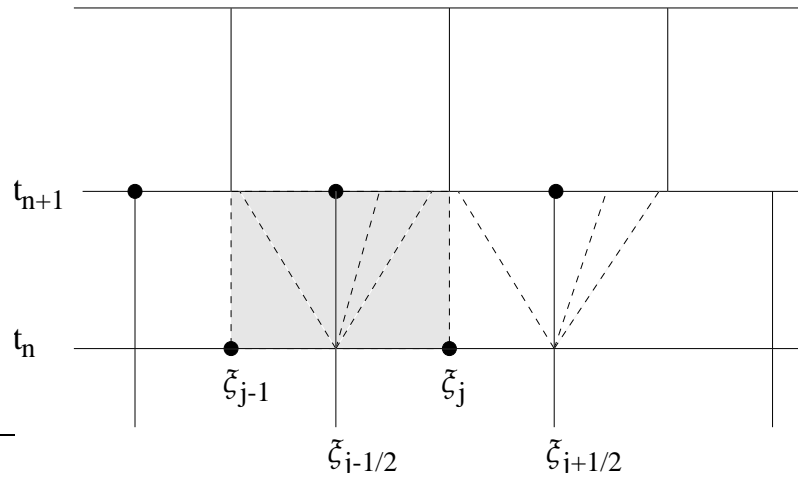


Figure 2: Staggered grid in space-time used in the NT scheme.

Remark 3.1. For piston problems it is important to use a variable time step, chosen close to the limit of the CFL stability condition,

$$\Delta t^n = c \frac{\Delta \xi}{\max_j \lambda_j^n}, \tag{3.2}$$

where c is the Courant number, $\lambda_j^n = \sqrt{\gamma_j^n p_j^n / V_j^n}$ denotes the sound speed at the j -th cell and time t^n , and $c \leq 1/2$ for stability reasons. Because of the compression of the system, the sound speed can change of an order of magnitude, and if a suitable time step is not used then the scheme becomes inefficient and inaccurate.

3.2 Is second order really second order?

In this section we discuss some implementation details which are important to guarantee that the Lagrangian scheme for the piston problem is effectively second order in space and time.

(a) Initial conditions.

In general, initial data are given in Eulerian coordinates:

$$\rho(x,0) = \rho_0(x), \quad (3.3a)$$

$$p(x,0) = p_0(x), \quad (3.3b)$$

$$u(x,0) = u_0(x), \quad (3.3c)$$

for $x \in [0, L(0)]$.

Given the data (3.3) one first computes the maximum Lagrangian coordinate

$$\xi_{\max} = \int_0^{L(0)} \rho_0(z) dz,$$

with a quadrature formula which is at least second order accurate. Then one defines $\Delta\xi = \xi_{\max}/J$, and computes the new coordinates x_j of the Eulerian grid at initial time:

$$\begin{aligned} x_0 &= -\Delta\xi/2\rho_0(0) \\ \text{for } j &= 0, 1, \dots, J \\ V_j &= 1/\rho_0(x_j) \\ u_j &= u_0(x_j) \\ \mathcal{E}_j &= u_j^2/2 + V_j p_0(x_j)/(\gamma-1) \\ x^* &= x_j + V_j \Delta\xi \\ V^* &= 1/\rho_0(x^*) \\ x_{j+1} &= x_j + \Delta\xi(V_j + V^*)/2 \\ \text{end} \end{aligned}$$

The correction in the computation of the Eulerian coordinates x_j ensures second order accuracy in the assignment of the initial data. Note that initial data are assigned also on the two ghost cells near the boundary, centered at x_0 and x_{J+1} .

(b) Boundary conditions and piston motion.

Boundary conditions can be assigned either at every time step or just at even time steps. In both cases, suitable values are defined on a number of ghost cells, that depends on the limiter which is used for the reconstruction of the derivatives. For example, in the case of the UNO limiter (3.1), three or five ghost cells are needed at even time steps, see Figs. 3-4. When boundary conditions are assigned at every time step, we compute the values of the field to three ghost cells at even times steps, and to two ghost cells at odd time steps (see Fig. 3).

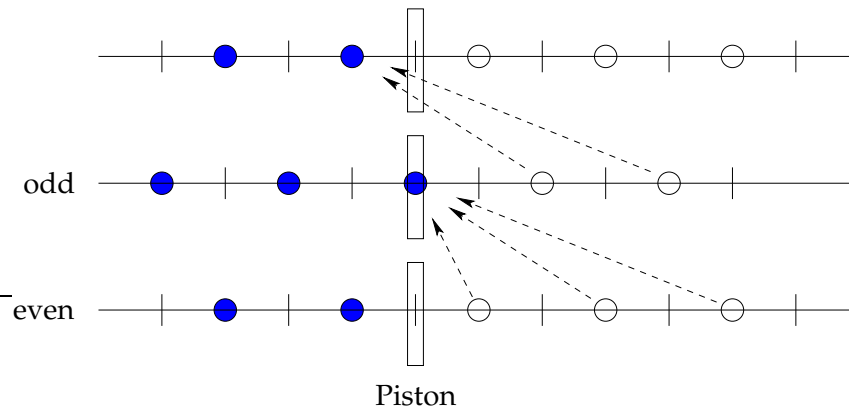


Figure 3: Three and two ghost cells (empty circles) are used at even and odd time steps, respectively. The field in the cell containing the piston at odd time step is computed in this way.

The values of the field at the cell containing the piston at odd time step is obtained as a result of the computation. When boundary conditions are assigned at even time steps only, the field is assigned at five ghost cells, and from it, it is computed on two ghost cells at odd time steps. In both cases, the field values at ghost cells are obtained by discretization of the boundary conditions illustrated in Section 2.3. More specifically, we assume that on the ghost cells the pressure profile is linear, with a slope equal to the acceleration of the piston; the entropy is assumed to be constant, and the velocity relative to the piston is an odd function, in a frame of reference with the origin on the piston.

For even time steps, this discretization can be treated as follows: the boundary condition for the pressure is discretized as

$$\frac{p_{J+1}^n - p_J^n}{\Delta \xi} = -a_p^n, \tag{3.4}$$

where a is the piston acceleration, the subscript p indicates a value at the piston. From the piston equation of motion, to second order, we have

$$a_p^n = \frac{A}{m} \left(\frac{p_J^n + p_{J+1}^n}{2} - p_{out} \right). \tag{3.5}$$

Substituting (3.5) into (3.4) and solving for p_{J+1} one finds the pressure at the first ghost cell $J+1$. The pressure at the other two ghost cells is computed as

$$p_{J+2+k}^n = 2p_{J+1+k}^n - p_{J+k}^n, \quad \text{for } k=0,1. \tag{3.6}$$

The specific volume V at the ghost cells is computed from the adiabaticity condition at the piston (2.13), that is described as

$$V_{J+k}^n = V_J^n (p_{J+k}^n / p_J^n)^{-1/\gamma}, \quad \text{for } k=0,1,2. \tag{3.7}$$

The velocity at the ghost cells is computed from the equations

$$\frac{u_{J+1+k}^n + u_{J-k}^n}{2} = u_p^n, \quad \text{for } k=0,1,2. \tag{3.8}$$

Analogous formulae hold for odd time steps n . The velocity of the piston, to second order, is computed by using trapezoidal rule

$$u_p^n = u_p^{n-1} + (a_p^n + a_p^{n-1}) \frac{\Delta t}{2}. \tag{3.9}$$

Naive boundary conditions are implemented by assuming a symmetric pressure and density distribution across the piston. For example, for even time steps, they are:

$$p_{J+1+k}^n = p_{J-k}^n, \quad V_{N+1}^n = V_N^n, \quad u_{J+1+k}^n = 2u_p^n - u_{J-k}^n, \quad \text{for } k=0,1,2. \tag{3.10}$$

As we shall see, using such boundary conditions cause degradation of the accuracy.

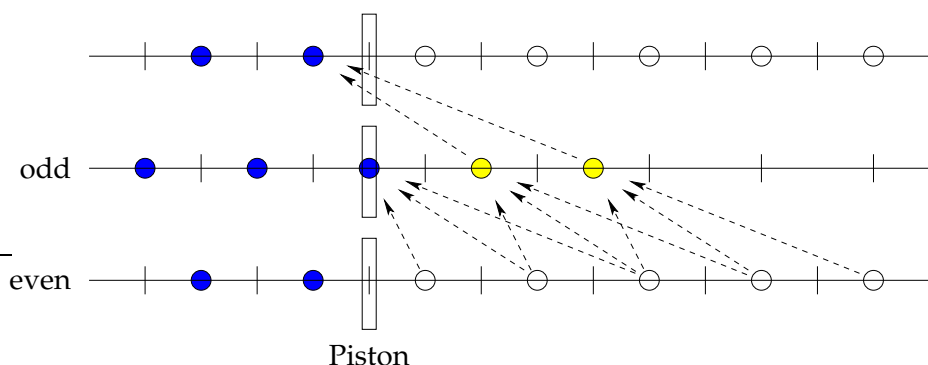


Figure 4: Five ghost cells (empty circles) are used at even time steps. The field in the cell containing the piston and two further ghost cells at odd time step are computed in this way.

When the boundary conditions on the ghost cells are assigned only at even time steps similar formulae can be derived by using the above assumptions. At the end of two time steps, after the field has been computed back on the original grid, two quantities have to be computed: the field at the five ghost cells (see Fig. 4) and the new velocity of the piston.

3.3 One gas convergence test

Here we perform some convergence test to be sure that our scheme is effectively second order accurate. We consider a single gas, that is $\gamma = \gamma_1 = \gamma_2 = 1.4$, and compute the solution at two different times, namely $t = 0.7$ and $t = 10$, using $J = 50, 100, 200, 400, 800, 1600$ cells.

The initial condition is a simple wave traveling with negative velocity

$$u(x,0) = \begin{cases} 0, & \text{if } |x-0.5| > \sigma, \\ -\theta\sqrt{\gamma} \left(1 + \cos\frac{\pi}{\sigma}(x-0.5)\right), & \text{otherwise,} \end{cases} \quad (3.11a)$$

$$\rho(x,0) = \left(1 - \frac{\gamma-1}{2\sqrt{\gamma}}u(x,0)\right)^{\frac{2}{\gamma-1}}, \quad (3.11b)$$

$$p(x,0) = \rho(x,0)^\gamma, \quad (3.11c)$$

with $\theta = 0.02$ and $\sigma = 0.3$. The piston conditions are given by

$$L(0) = 1, \quad \frac{dL}{dt}(0) = 0. \quad (3.12)$$

The remaining data are given by $A/m = 0.1, p_{out}(t) = 2$. UNO limiter (3.1) has been used in all numerical computation performed for this section.

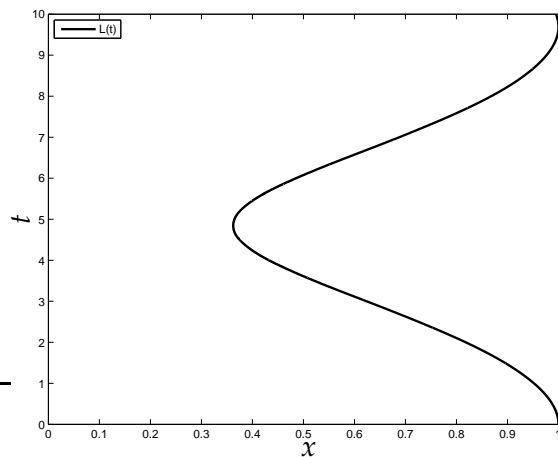


Figure 5: Piston position for $J = 200$.

As it is easily seen from Fig. 5, for the data shown above, the time $t = 10$ is close to a full oscillation of the piston, while at time $t = 0.7$ the piston has barely moved.

The convergence results (L_1 norm of the error and accuracy order) are summarized in Table 1. The errors for a field variable, say V , are computed as follows. First we compute the cell average of V on the coarsest grid, for all grids. For example, in order to compare $V^{(\Delta\xi)}$ with $V^{(2\Delta\xi)}$, we compute the absolute error as

$$\sum_{j=1}^{J_{2\Delta\xi}} \left| V_j^{(2\Delta\xi)} - \bar{V}_j^{(\Delta\xi)} \right|.$$

Here $V^{(\Delta\xi)}$ denotes the field V on the grid of cell size $\Delta\xi$, and $\bar{V}^{(\Delta\xi)} = (V_{2j}^{(\Delta\xi)} + V_{2j+1}^{(\Delta\xi)})/2$. Once all the averages are computed on the coarsest grid, then error and convergence rate

Table 1: Convergence test at time $t=0.7$. Relative error and convergence rate in V and in p . Second order boundary condition at the piston.

$J - 2J$	L_1 error and order in V		L_1 error and order in p	
50 - 100	5.77641E-05	1.7548	7.76363E-05	1.7865
100 - 200	1.71159E-05	1.7363	2.25052E-05	1.7302
200 - 400	5.13707E-06	1.5151	6.78333E-06	1.5463
400 - 800	1.79731E-06	1.9025	2.32246E-06	1.8990
800 - 1600	4.80758E-07	3.0337	6.22702E-07	3.1332
1600 - 3200	5.87075E-08	2.4472	7.09744E-08	2.4431
3200 - 6400	1.07647E-08		1.30516E-08	

are computed by the usual Richardson extrapolation technique:

$$V^{(\Delta\zeta)} = V + C\Delta\zeta^r + o(\Delta\zeta^r),$$

which gives

$$E^{(\Delta\zeta)} \approx V^{(2\Delta\zeta)} - \bar{V}^{(\Delta\zeta)} = C(2^r - 1)\Delta\zeta^r + o(\Delta\zeta^r).$$

Relative errors $e^{(\Delta\zeta)}$ are computed dividing $\|E^{(\Delta\zeta)}\|_1$ by $\|\bar{V}^{(\Delta\zeta)}\|_1$. Finally, the convergence rate r is estimated as

$$r \approx \log\left(\frac{e^{(2\Delta\zeta)}}{e^{(\Delta\zeta)}}\right) / \log 2.$$

Fig. 6 show the bestfit of the absolute L_1 error in logarithmic scale, both for V and p . The slopes of the two curves are, respectively, -2.034 and -2.060 , indicating a second order convergence rate.

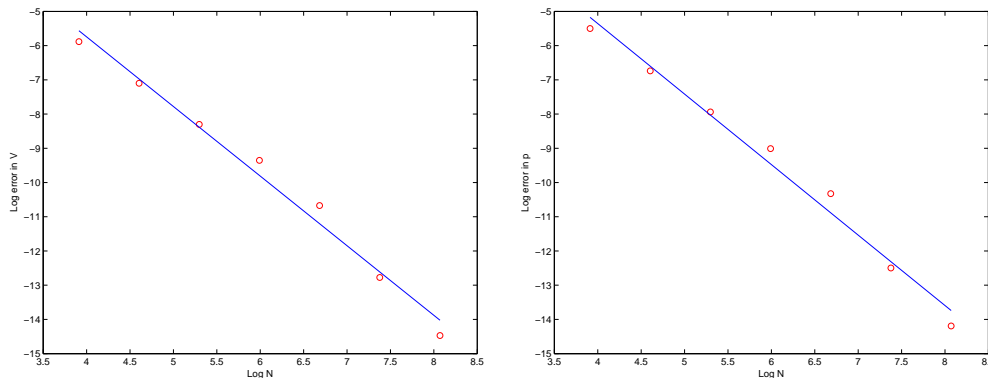


Figure 6: Best fit in logarithmic scale of the error as a function of the grid size, for the computation with second order boundary conditions and final time $t=0.7$

Pressure profile for this test are shown in Figs. 7, 8 and 9. The same test has been repeated, using naive boundary conditions at the piston, and the results are reported in

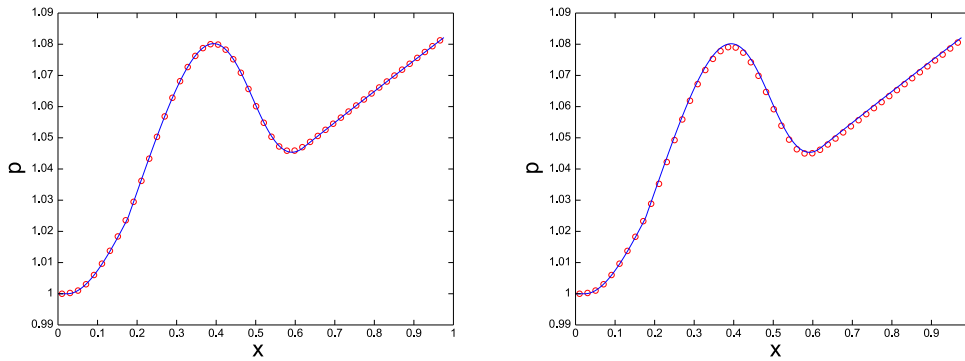


Figure 7: Pressure profile at time $t=0.7$ for $J=50$ (circle) and $J=1600$ (solid line). Left: second order boundary condition at the piston. Right: naive boundary conditions at the piston.

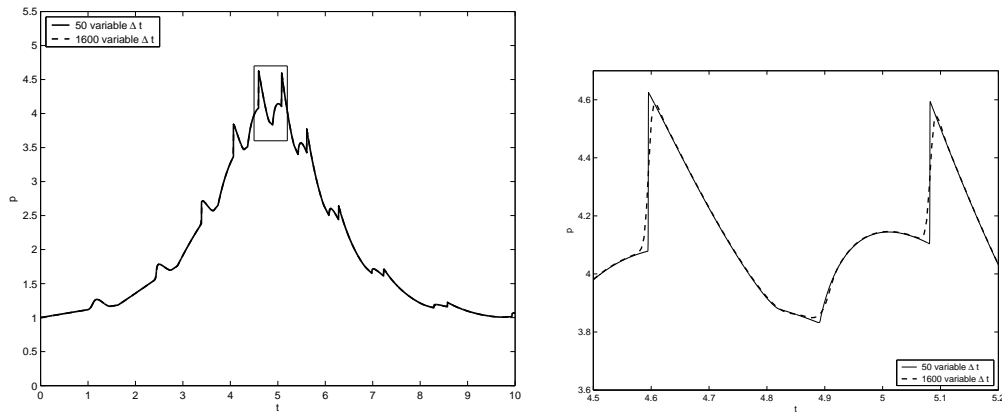


Figure 8: Pressure history at the piston for $J=50$ dashed line and $J=1600$ solid line. Left: Pressure evolution at the piston up to time $t=10$. Right: zoom for the range $t \in [4.5, 5.2]$.

Table 2: Convergence test at time $t=0.7$. Relative error and convergence rate in V and in p . Naive boundary conditions at the piston.

$J - 2J$	L_1 error and order in V		L_1 error and order in p	
50 - 100	2.52977E-04	1.0023	3.59824E-04	1.004
100 - 200	1.26284E-04	1.0128	1.79392E-04	1.008
200 - 400	1.29983E-04	1.0052	1.77262E-04	1.005
400 - 800	3.11800E-05	1.0203	4.44382E-05	1.017
800 - 1600	1.53722E-05		2.19585E-05	

Table 2. In Fig. 8 we plot the time evolution of the pressure at the piston up to the time $t=10$. The spikes in the pressure profile occur when the shock wave reaches the piston. Fig. 9 shows the space distribution of the pressure at time $t=10$, which corresponds to a full oscillation of the piston. Both second order boundary condition and the naive

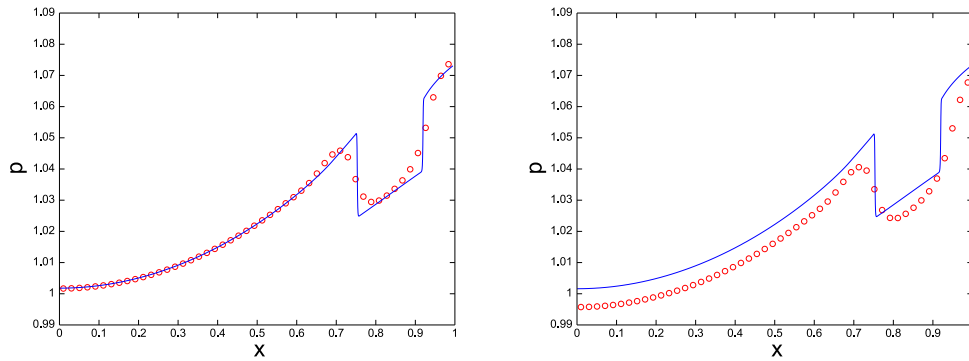


Figure 9: Pressure profile at time $t=10$ for $J=50$ (circle) and $J=1600$ (solid line). Left: second order boundary condition at the piston. Right: naive boundary conditions at the piston.

boundary condition at the piston are illustrated. As it is evident from the above tables and figures, our scheme gives the expected second order accuracy before interaction, and it gives more than first order accuracy (in L_1 norm) after a long time. Also, the use of the naive boundary conditions degrades the accuracy of the scheme. However, by comparing the reference solutions, namely the ones with 1600 cells, we can notice that in both cases convergence to the same reference solution is achieved as $\Delta x \rightarrow 0$.

The accuracy is degraded also if a first order scheme is used for the time evolution of the piston. The five point ghost cells treatment at the boundary has given similar results to the above treatment. We have not reported here the numerical results for the sake of brevity.

4 Balancing the pressure at the interface

The development of this section starts from the observation that, due to the presence of the interface, several quantities (such as density and energy) may be discontinuous, but pressure and velocity have to be continuous across the interface. This condition is enforced in our scheme.

As stated above, being a material line, the interface moves with the velocities of the two gases (which are equal there). Using this condition, together with the jump relations across a discontinuity (also known as Rankine-Hugoniot conditions, see Whitham [24]) imposed at the interface we get that p does not jump at the interface, unless we take into account the effect of surface tension. On the other hand, we may suppose that there are two different gases across the interface, with different physical properties. In particular, the molecular mass of the two gases may be different, and in this case there would be a jump in the density, even if temperature and pressure are continuous.

We shall consider problems in which the interface is initially located exactly between two adjacent cells. This is obtained with a suitable choice of the grid. After one time step,

the interface will be located in the middle of a cell (see Fig. 2). The field variables ($\rho, \rho u, E$ in Eulerian coordinates or V, u, \mathcal{E} in Lagrangian coordinates) in the middle cell represent some average of the corresponding field variables on the two sides of the interface.

A key feature of the numerical scheme is that it should maintain static solutions. This means that if the initial data represents a static state, it should be unchanged after two time steps. This can be obtained by defining a suitable formula for the pressure of the interface cell, and by a suitable reconstruction of the field variables on the two sides of the interface.

At the initial time we assume that the interface is located at the boundary between cell j_w and cell $j_w + 1$. Because of the use of Lagrangian coordinates, the interface will always separate cell j_w from cell $j_w + 1$ at even time steps, and it will be in the middle of cell $j_w + 1/2$ at odd time steps (see Fig. 10).

Let us denote by subscript 1 and 2 the values of the field variables on the two sides of the interface cell at odd time steps. The balance of the pressure on the two sides of the interface, $p_1 = p_2$, gives

$$\frac{\gamma_1 - 1}{V_1} \left(\mathcal{E}_1 - \frac{1}{2} u^2 \right) = \frac{\gamma_2 - 1}{V_2} \left(\mathcal{E}_2 - \frac{1}{2} u^2 \right). \quad (4.1)$$

We assume that on the two sides of the interface there are two different gases, and we denote by η the ratio of the densities on the two sides

$$V_2 = \eta V_1. \quad (4.2)$$

From perfect gas law, it follows that if the temperature is continuous across the interface, then η is given by the ratio of the molecular masses of the two gases. However, to assume that the temperature does not jump at the interface is not strictly correct. Such an approximation is a good one only for low amplitude waves, or when the two gases have almost the same polytropic constant, but may not be appropriate in others cases. For example when a strong shock crosses an interface of two very different gases, it produces a strong jump in the temperature. This is not surprising, since Euler equations do not react to a temperature jump, because they are inviscid, and there is no heat conduction. We shall call this interface condition the *isothermal condition*. The approximation here is similar to the one present in standard shock capturing schemes when dealing with a contact discontinuity. Across a contact discontinuity on a single gas there is a temperature jump. A shock capturing central schemes that is not specially designed to deal with contact will smear it out over a certain number of cells, which depends on the numerical viscosity of the scheme. Here something similar will happen: the contribution of the discontinuity due to the difference in the molecular mass is automatically taken care by the scheme, but the additional contribution due to the jump in temperature will be smeared.

In general, if we assume that the temperature ratio across the interface is constant in time, then η will be constant, and equal to the initial density ratio. In fact, from the perfect gas law one has:

$$p_i = R_i \rho_i T_i, \quad i = 1, 2,$$

where T denotes the absolute temperature, $R_i = R/m_i^*$ are the gas constant per unit mass, and m_1^* and m_2^* are the molecular weights of the two gases. From $p_1 = p_2$, it follows

$$\eta = \frac{\rho_1}{\rho_2} = \frac{T_2 m_1^*}{T_1 m_2^*} = \frac{V_2}{V_1}.$$

The cell average of the specific volume V and energy \mathcal{E} at the interface cell $j_w + 1/2$ are computed by integrating the piecewise linear reconstruction at the two cells near the interface:

$$\bar{V} = \frac{\bar{V}_1 + \bar{V}_2}{2} + \frac{1}{2} V_1' + V_2' \Delta \xi = \frac{V_1 + V_2}{2} + \frac{3}{8} V_2' - V_1' \Delta \xi$$

and similar formula for the energy. Here V_1 and V_2 denote the pointwise values at the interface, and V_1' and V_2' denote the slopes in the profiles in the two cells adjacent to the interface. As it is usually done in central schemes, we identify pointwise values in the cell center with the cell average, obtaining the expressions

$$V = \frac{V_1 + V_2}{2}, \quad \mathcal{E} = \frac{\mathcal{E}_1 + \mathcal{E}_2}{2}. \quad (4.3)$$

Note that these approximations are second order accurate only if the slopes on the two sides differ by terms of $\mathcal{O}(\Delta \xi)$. Here, because of the discontinuity at the interface, such an assumption is not necessarily verified, and this may reduce the accuracy of the approximation.

Making use of above relations (4.1)-(4.3) we get the following formula for the pressure $p = p_1 = p_2$ in terms of the field variables at the interface

$$p(V, u, \mathcal{E}) = \frac{(1+\eta)(\gamma_1-1)(\gamma_2-1)}{\eta\gamma_1 + \gamma_2 - 1 - \eta} \left(\mathcal{E} - \frac{1}{2} u^2 \right) / V, \quad (4.4)$$

where in the isothermal condition

$$\eta = \frac{\rho_1(x_{j_w}, 0)}{\rho_2(x_{j_w}, 0)} = \frac{V_2(x_{j_w}, 0)}{V_1(x_{j_w}, 0)}.$$

Note that by setting $\eta = 1$ and $\gamma_1 = \gamma_2 = \gamma$ we recover from (4.4) the classical equation of state for a polytropic gas.

Once the interface quantities are known, the values of the field variables on the two sides can be computed

$$\begin{aligned} V_1 &= \frac{2}{1+\eta} V, & \mathcal{E}_1 &= \frac{p(V, u, \mathcal{E}) V_1}{\gamma_1 - 1} + \frac{1}{2} u^2, \\ V_2 &= \frac{2\eta}{1+\eta} V, & \mathcal{E}_2 &= \frac{p(V, u, \mathcal{E}) V_2}{\gamma_2 - 1} + \frac{1}{2} u^2. \end{aligned} \quad (4.5)$$

Fig. 10 shows the evolution of the specific volume obtained by our scheme on two time steps for a steady solution. A similar picture is obtained for the evolution of the energy. Note how the scheme maintains static solutions.

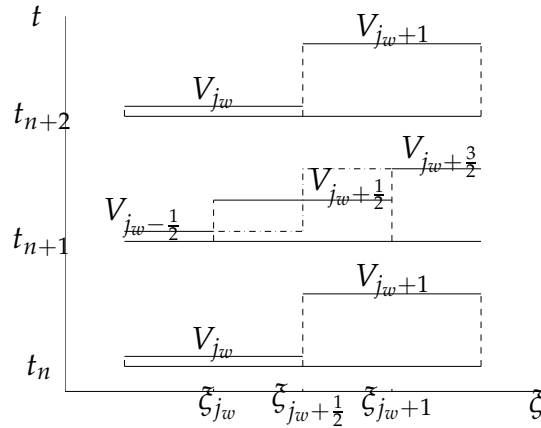


Figure 10: Evolution of the specific volume V near the interface cell for a steady solution. The results are obtained by our scheme.

5 Two gas numerical tests

In this section we report several numerical tests performed in order to validate the Lagrangian scheme.

All the quantities are represented using the more familiar Eulerian coordinate x rather than ξ . The Eulerian coordinate of the center of cell k (at even time steps) is obtained by a discrete version of Eq. (2.8),

$$x_k = \Delta \xi \left(-\frac{1}{2} V_1 + \sum_{j=1}^k V_j \right).$$

We used MinMod limiter (3.1) in all numerical test performed in this section.

5.1 Piston problem

The first model we consider is related to the physical setup of two gases separated by an interface between a solid wall and a plane piston (see Fig. 1).

We perform three tests, with different values of γ . Two tests represents in fact a single fluid, with polytropic constant $\gamma_1 = \gamma_2 = 1.4$ and $\gamma_1 = \gamma_2 = 1.667$. In the third test there are two fluids with $\gamma_1 = 1.4$ and $\gamma_2 = 1.667$.

The related initial and interface conditions are as follows

$$(\rho, u, p) = \begin{cases} (\rho_1, u_1, p_1) = (1.0, 0.0, 1.0), & 0 \leq x \leq I(0), \\ (\rho_2, u_2, p_2) = (1.0, 0.0, 1.0), & I(0) \leq x \leq L(0), \end{cases} \quad (5.1a)$$

$$I(0) = 0.5, \quad L(0) = 1, \quad \frac{dL}{dt}(0) = 0, \quad (5.1b)$$

$$\frac{dI}{dt}(t) = u_1(I(t), t) = u_2(I(t), t), \quad (5.1c)$$

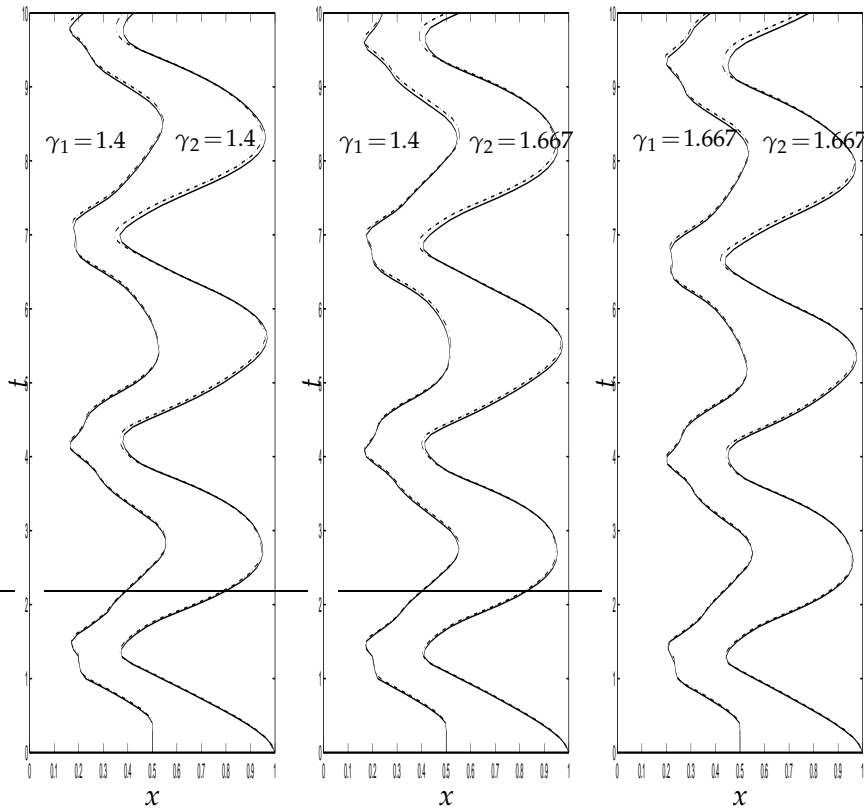


Figure 11: Numerical test for Eulerian and Lagrangian schemes: left $\gamma_1 = \gamma_2 = 1.4$, middle $\gamma_1 = 1.4, \gamma_2 = 1.667$ and right $\gamma_1 = \gamma_2 = 1.667$. Solid lines Eulerian scheme with 100 grid points. Dashed-dotted lines Lagrangian central scheme with 100 grid points.

the remaining data are given by $A/m=2, p_{out}(t)=2$. For this test we applied the isothermal condition $\eta=1$ at the interface.

Fig. 11 illustrates a comparison of numerical results. We plot the evolution of the interface and the piston with time, in the three cases, obtained with two completely different methods. One is the central Lagrangian method described in this paper. The other is an upwind-based Eulerian scheme which adopts a moving mesh approach, proposed by Fazio and LeVeque [8]. The agreement of the two approaches is remarkable, considering that only 100 grid points have been used.

In the initial condition the two gases are at rest, with constant pressure throughout the domain. The piston is set into motion by the (positive) difference between external and internal pressure.

Observe that the interface does not move for a while. It starts moving when the acoustic waves propagating inward from the piston reach it.

The motion of the system is oscillatory. The case on the left shows slightly more than 3.5 periods up to the final time $t=10$, while the case on the right shows almost 4 full

periods. As expected, the period of oscillation for the $\gamma = (1.4, 1.4)$ case is slightly larger than the period for the $\gamma = (1.667, 1.667)$ case, because in the latter case the gas is slightly stiffer and reacts more promptly to the pressure difference. The behavior of the system with two gases, $\gamma_1 = 1.4$, $\gamma_2 = 1.667$, is intermediate between the previous two.

This is an academic example, which is used for the purpose of comparing two different numerical approaches. In a more realistic simulation one should use different densities for the initial condition of the two gases. However, in that case a comparison with the two single gas calculation can not be made.

5.2 Adiabatic approximation

In this subsection we consider the adiabatic approximation for the piston problem of Section 2.1. This test was presented at the eight international hyperbolic conference held in Magdeburg in 2000 [9].

In the adiabatic approximation the piston moves at a velocity which is much lower than the sound speed. As a result, for appropriate initial conditions, the pressure can be considered constant in the whole domain, and depends only on time. Furthermore, the entropies of both gases are constants, equal to their initial values. The above conditions alone are enough to describe the motion of the interface and of the piston by a single ordinary differential equation of second order. The above approximation is a good one for a sufficiently heavy piston.

The equation of motion can be obtained as follows. Because the motion is adiabatic, the evolution of the gas is isentropic, and the pressures of the two gases are given by

$$p_1 = k_1 \rho_1^{\gamma_1}, \quad p_2 = k_2 \rho_2^{\gamma_2}.$$

The densities of each gas are constant in space, and they are inversely proportional to the length of the corresponding region. We can therefore write

$$p_1 = \tilde{k}_1 I^{-\gamma_1}, \quad p_2 = \tilde{k}_2 (L - I)^{-\gamma_2},$$

where \tilde{k}_1 and \tilde{k}_2 are some constants that depend on the initial conditions.

By equating the pressures one can solve for L

$$L = I + c_1 I^\varrho, \tag{5.2}$$

where $\varrho = \gamma_1 / \gamma_2$. The constant c_1 can be determined from the initial conditions

$$c_1 = (L_0 - I_0)(I_0)^{-\varrho}.$$

The equation of motion for the piston is

$$\frac{d^2 L}{dt^2} = \frac{A}{m} (p(t) - p_{\text{out}}(t)).$$

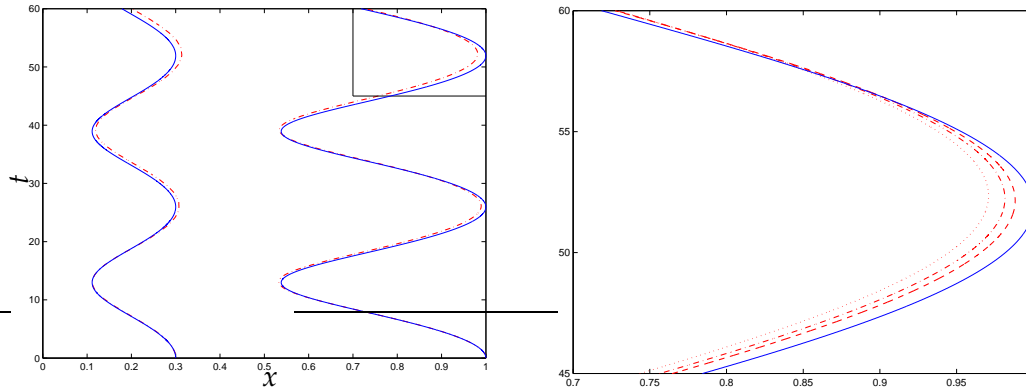


Figure 12: Adiabatic approximation, left: interface and piston positions in the x - t plane, dashed line: adiabatic solution, solid line: numerical solution with 200 mesh-cells; right: detail of the piston position for 100, 200, and 400 mesh-cells.

Differentiating Eq.(5.2), and using the relation for the pressure $p = p_0(I/I_0)^{-\gamma_1}$, one obtains the following equation for I

$$\frac{d^2 I}{dt^2} (1 + c_1 \varrho I^{\varrho-1}) + c_1 \varrho (\varrho - 1) I^{\varrho-2} \left(\frac{dI}{dt} \right)^2 = \frac{A}{m} (c_2 I^{-\gamma_1} - p_{out}(t)), \quad (5.3)$$

with $c_2 = p_0 I_0^{\gamma_1}$, and p_0 is the initial pressures on both sides of the interface. The piston position can be obtained from the interface position via the relation

$$L(t) = (L(0) - I(0)) \left(\frac{I(t)}{I_0} \right)^\varrho + I(t).$$

We solve Eq. (5.3) with the following data $L(0) = 1$, $p_0 = 1$, $A/m = 0.01$, $p_{out}(t) = 2$, $\gamma_1 = 1.4$, $\gamma_2 = 1.667$, and initial conditions

$$I(0) = 0.3, \quad \frac{dI}{dt}(0) = 0,$$

and then we solve Eq. (2.5) with the same data and initial conditions

$$(\rho, u, p) = \begin{cases} (\rho_1, u_1, p_1) = (1.0, 0.0, 1.0), & 0 \leq x \leq I(0), \\ (\rho_2, u_2, p_2) = (1.0, 0.0, 1.0), & I(0) \leq x \leq L(0). \end{cases}$$

The position of the interface is computed from the numerical solution by solving the equation

$$\frac{dI}{dt}(t) = u_1(I(t), t) = u_2(I(t), t).$$

Fig. 12 shows the good agreement between the adiabatic approximation and the numerical results obtained by our central scheme by setting $\Delta \xi = 0.005$, that is 200 mesh points. A Courant number $\mu \max_j \rho(A(\mathbf{q}_j^n)) = 0.45$ has been used. Note that the average sound speed is around 2, so during the displayed time span the acoustic waves go back and forth between the piston and the wall more that 50 times.

5.3 Shock-interface interaction

The physical setup for the test, as shown in Fig. 13, is to consider the interaction of a shock moving from left to right towards the interface. The tube is supposed to be open at both sides, and consequently inflow (outflow) boundary conditions at the left (right) boundary are provided.

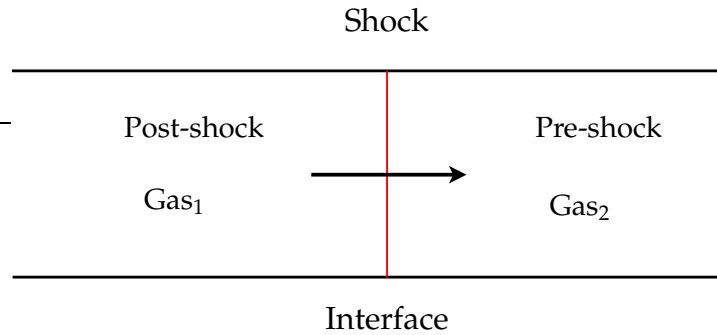


Figure 13: Physical setup for shock-interface problems.

The test problem considered here is the one studied by Abgrall and Karni [3]. They consider the following initial conditions (see [3], Test case 4):

$$\begin{aligned} (\rho_1, u_1, p_1) &= (1.0, 0.0, 500.0), & 0 \leq x < I(0), \\ (\rho_2, u_2, p_2) &= (1.0, 0.0, 0.2), & I(0) < x \leq L(0) = 1, \end{aligned} \tag{5.4}$$

with $I(0) = 0.5$, $A = 0$ (that is $L(t) = 1$), $\gamma_1 = 1.4$ and $\gamma_2 = 1.6$.

Fig. 14 illustrates the numerical results for the shock-interface interaction problem. This can be compared with those reported in Fig. 6 of [3] where 800 grid points were used. We notice that our results are free from the slight overshoots observed by those authors at the corner of the rarefaction fan.

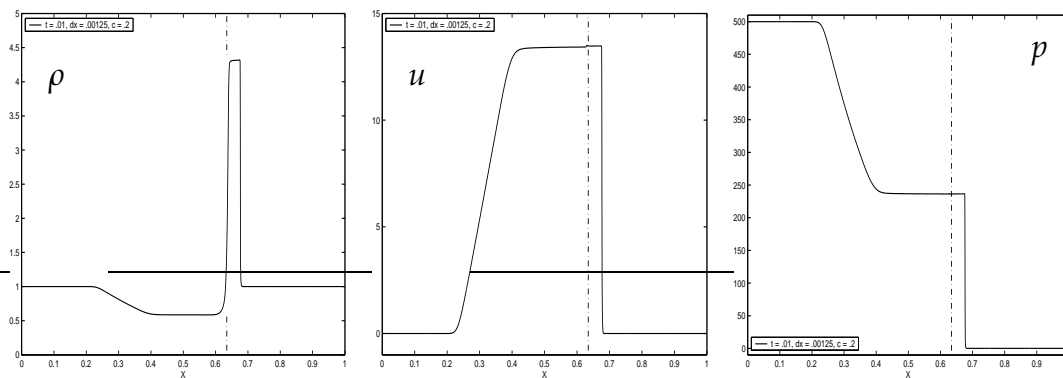


Figure 14: Abgrall-Karni Test 4. Numerical results at $t = 0.01$ computed with 800 mesh cells. Left: density. Center: velocity. Right: pressure.

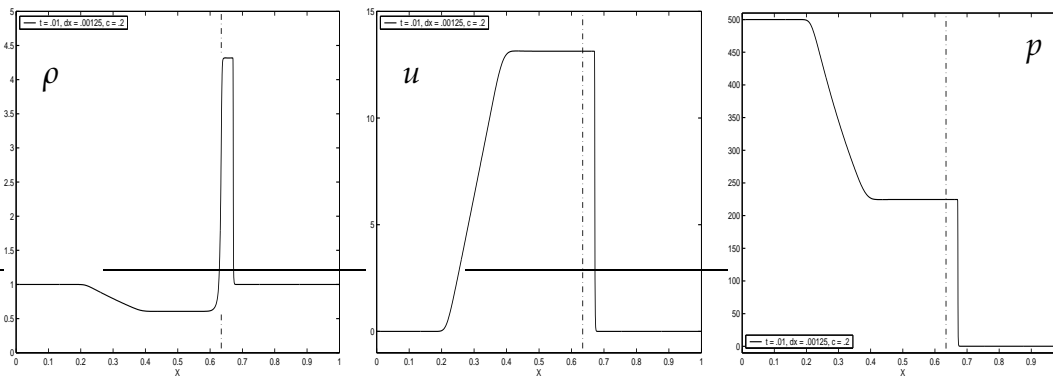


Figure 15: One fluid test with initial data (5.4) and 800 mesh cells, but with $\gamma = 1.6$. Left: density. Center: velocity. Right: pressure.

In Fig. 15 the calculation is repeated with a single gas with $\gamma = 1.6$. Note that the qualitative behavior of the two cases is very similar. The lack of resolution at the interface is not due to our treatment of the interface, but rather to the relatively poor performance of central schemes (with no artificial compression) at contact discontinuities, when compared to upwind schemes. The computations for this test have been performed with a Courant number 0.2, which does not show the small oscillations present when using larger values (e.g. 0.45).

Better results on this test case could be obtained using the so called "artificial compression method" of Harten [11], suitably adapted to central schemes by Lie and Noelle [17].

6 Conclusions

In this paper we develop a staggered fully conservative central scheme for multi-fluid flows in Lagrangian coordinates. The central scheme does not require the solution to exact or approximate Riemann problems. Furthermore, by using Lagrangian coordinates, we do not require the use of additional equations for the interface motion, as is done, for example, with level set or mass fraction models. The main contribution is the derivation of a special equation of state to be imposed at the interface in order to avoid non-physical oscillations. For the piston problem we describe two different ways to impose boundary conditions at the piston, that ensure second order convergence.

The proposed scheme is validated by solving several tests concerning one-dimensional hyperbolic interface problems. In particular we compare our results with: a moving mesh reference solution for a piston problem, a reference solution obtained by accurately solving a second order ordinary differential equation describing the equation of motion of the piston in the adiabatic approximation, and a benchmark shock-interface interaction problem. The agreement of the solutions obtained by the present method with those available

in the literature shows the effectiveness of the proposed approach.

The main limitation of the present Lagrangian approach is that it is difficult to extend it to multi-dimensional problems. This difficulty can be overcome by using Eulerian formulation with moving mesh, similar to the one used in [8] for one dimensional problems. If the interface can be described, for instance in 2D, by a function $x_s = x_s(y, t)$, then the moving mesh can be effectively used by moving the mesh only in the x -direction. A similar approach to the treatment of interfaces in 2D flows is used, for example, by Le Duc et al. [6]. A moving mesh Eulerian scheme with second order boundary conditions and its extension to problems in two space dimension is presently under investigation.

Acknowledgments

The research of this work was supported by grants of the Catania and Messina Universities and partially by the Italian "MIUR".

References

- [1] R. Abgrall. Generalization of the Roe scheme for the computation of mixture of perfect gases. *Rech. Aérop.*, 6:31–43, 1988.
- [2] R. Abgrall. How to prevent pressure oscillations in multicomponent flow calculations: a quasi conservative approach. *J. Comput. Phys.*, 125:150–160, 1996.
- [3] R. Abgrall and S. Karni. Computation of compressible multifluids. *J. Comput. Phys.*, 169:594–623, 2001.
- [4] D. J. Benson. Computational methods in Lagrangian and Eulerian hydrocodes. *Comput. Methods Appl. Mech. Engrg.*, 99:235–394, 1992.
- [5] S. F. Davis. An interface tracking method for hyperbolic systems of conservation laws. *Appl. Numer. Math.*, 10:447–472, 1992.
- [6] A. Le Duc, J. Sesterhenn, and R. Friedrich. Instabilities in compressible attachment-line boundary layers. *Phys. Fluids*, 18:044102–16, 2006.
- [7] R. Fazio. Comparison of two conservative schemes for hyperbolic interface problems. In F. Brezzi, A. Buffa, and A. Murli, editors, *Numerical Mathematics and Advanced Applications*, pages 85–93. Springer-Italia, Milano, 2003.
- [8] R. Fazio and R. J. LeVeque. Moving-mesh methods for one-dimensional hyperbolic problems using CLAWPACK. *Comp. & Math. Appl.*, 45:273–398, 2003.
- [9] R. Fazio and G. Russo. Eulerian and Lagrangian schemes for hyperbolic interface problems. In H. Freistühler and G. Warnecke, editors, *International Series of Numerical Mathematics*, volume Vol. 140, pages 347–356, 2001. Eighth International Conference on Hyperbolic Problems, Theory, Numerics, Applications, Magdeburg, 28 February - 3 March, 2000.
- [10] R. P. Fedkiw, T. Aslam, B. Merriman, and S. Osher. A non-oscillatory eulerian approach to interfaces in multimaterial flows (the ghost fluid method). *J. Comput. Phys.*, 152:457–492, 1999.
- [11] A. Harten. The artificial compression method for computation of shocks and contact discontinuities. i. single conservation laws. *Comm. Pure Appl. Math.*, 30:611–638, 1977.
- [12] A. Harten, B. Engquist, S. Osher, and S. Chakravarthy. Uniformly high order accurate essentially non-oscillatory schemes III. *J. Comput. Phys.*, 71:231–303, 1987.

- [13] S. Karni. Hybrid multifluid algorithms. *SIAM J. Sci. Comput.*, 17:1019–1039, 1996.
- [14] A. Kurganov, S. Noelle, and G. Petrova. Semidiscrete central-upwind schemes for hyperbolic conservation laws and Hamilton-Jacobi equations. *SIAM J. Sci. Comput.*, 23(3):707–740 (electronic), 2001.
- [15] A. Kurganov and E. Tadmor. New high-resolution central schemes for nonlinear conservation laws and convection-diffusion equations. *J. Comput. Phys.*, 160(1):241–282, 2000.
- [16] B. Larouturou. How to preserve the mass fraction positive when computing compressible multi-component flows. *J. Comput. Phys.*, 95:59–84, 1991.
- [17] K.-A. Lie and S. Noelle. On the artificial compression method for second-order nonoscillatory central difference schemes for systems of conservation laws. *SIAM J. Sci. Comput.*, 24:1157–1174, 2003.
- [18] B. Lombard and R. Donat. The explicit simplified interface method for compressible multi-component flows. *SIAM J. Sci. Comput.*, 27:208–230, 2005.
- [19] W. Mulder, S. Osher, and J. Sethian. Computing interface motion: The compressible Rayleigh-Taylor and Kelvin-Helmholtz instabilities. *J. Comput. Phys.*, 100:209–228, 1992.
- [20] H. Nessyahu and E. Tadmor. Non-oscillatory central differencing for hyperbolic conservation laws. *J. Comput. Phys.*, 87:408–463, 1990.
- [21] S. Osher and R. P. Fedkiw. *Level set methods and dynamic implicit surfaces*. Springer-Verlag, New York, 2003.
- [22] E. H. van Brummelen and B. Koren. A pressure-invariant conservative Godunov-type method for barotropic two-fluid flows. *J. Comput. Phys.*, 185:289–308, 2003.
- [23] H. Wang, M. Al-Lawatia, and R. C. Sharpley. A characteristic domain decomposition and space-time local refinement method for first-order linear hyperbolic equations with interfaces. *Numer. Meth. Partial Differential Equations*, 15:1–28, 1999.
- [24] G. B. Whitham. *Linear and nonlinear waves*. Wiley, New York, 1974.